



Optical diffraction radiation from a dielectric and a metal nanowire excited by a modulated electron beam

Dariia O. Yevtushenko^{1,2} · Sergii V. Dukhopelnykov² · Alexander. I. Nosich²

Received: 16 October 2018 / Accepted: 27 December 2018
© Springer Science+Business Media, LLC, part of Springer Nature 2019

Abstract

The optical diffraction radiation that accompanies the motion of a modulated beam of electrons near a dielectric and silver nanowire scatterers is investigated in the two-dimensional formulation. Our goal is to compute the field in the near and far zones and analyze how it depends on electron beam parameters. We demonstrate the excitation of internal resonances of such a scatterer that can be useful in the design of nanoscale non-invasive beam position monitors.

Keywords Diffraction radiation · Nanowire scatterers · Smith–Purcell effect · Surface wave · Plasmon resonance · Total scattering cross-section · Absorption cross-section

1 Introduction

As known, charged particles, such as electrons, radiate electromagnetic waves when moving through the boundary between material media—this is called the transition radiation. The radiation of electrons moving in vacuum without crossing any material boundaries has also attracted the attention of researchers. The most known example of such effect is the Smith–Purcell radiation (Smith and Purcell 1953; van den Berg 1973; Nosich 1981; Veliev et al. 1977; Castellano 1997; Potylitsyn 1998; Castellano et al. 2001; Karataev et al. 2004; Goponov et al. 2018; Bobb et al. 2018; Baryshevsky and Gurnevich 2017; Talebi 2017; Leedle et al. 2015); it is associated with an electron beam flowing over a periodic grating, for instance, ruled on a metal surface. Still the Smith–Purcell radiation is only a particular case of more general phenomenon: the radiation of the surface and polarization currents induced on the metal and dielectric objects by the electron beams flowing in their vicinity however without touching them. This type of electromagnetic-wave radiation is commonly called the *diffraction radiation* (DR) (Nosich 1981; Veliev et al. 1977; Castellano 1997; Potylitsyn 1998; Castellano et al. 2001; Karataev et al. 2004; Goponov et al. 2018; Bobb

✉ Dariia O. Yevtushenko
dariia.yevtushenko@gmail.com

¹ Department of Photonics and Laser Engineering, Kharkiv National University of Radio Electronics, Kharkiv 61066, Ukraine

² Laboratory of Micro and Nano Optics, Institute of Radio-Physics and Electronics NASU, Kharkiv 61085, Ukraine

et al. 2018; Baryshevsky and Gurnevich 2017; Talebi 2017; Leedle et al. 2015). DR of the microwave range finds application in the design of beam position monitors of various particle accelerators. As known, the characteristics of such monitors can be enhanced if the scatterers are shaped as cavities, thanks to the associated high-Q resonances (Nosich 1981).

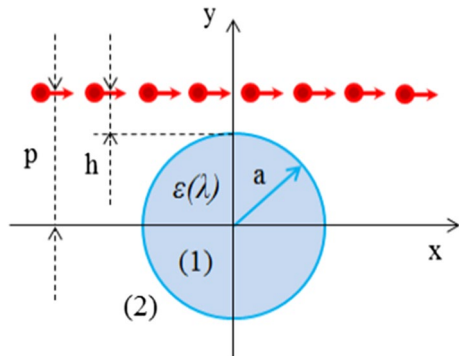
Detection of DR in the visible wavelength range, called the optical DR, is the most promising technique for application to noninvasive beam diagnostics (Potylitsyn 1998; Castellano et al. 2001; Karataev et al. 2004; Goponov et al. 2018; Bobb et al. 2018). Here, the emergence and rapid development of nanotechnologies opens the way to use nanoscale scatterers as sensitive antennas (Baryshevsky and Gurnevich 2017; Talebi 2017). Indeed, such antennas radiate the optical waves, characterized with the far-field patterns and the carried power values depending on the electron-beam bunching, velocity, and fine distance to the beam trajectory. For instance, for the configuration in Fig. 1, the measurement of the DR pattern can deliver the information on the beam position shift h and velocity v .

Note that the nanowires can be designed resonant and, moreover, tunable by covering the wires with the graphene (Leedle et al. 2015; Bohren and Huffman 2004; Velichko and Natarov 2018). Nanoscale size of such beam-sensor antennas introduces negligible distortion to the beam energy characteristics, which can be considered as fixed. This makes possible the analysis of sensing antenna elements in the same way as within the traditional antenna theory, i.e. as the scattering of the given electromagnetic field of the moving beam by the conducting and dielectric scatterers of given shapes and material properties. The latter parameters can be manipulated to optimize the beam-diagnostics antenna performance.

Such scatterers can be also designed to display the resonances from ultraviolet to infrared wavelengths. The associated resonances are then either on the low-order internal modes of dielectric objects or the localized surface plasmon (LSP) modes of noble-metal objects (Bohren and Huffman 2004; Velichko and Natarov 2018). Note that the plasmonic scatterers can be designed tunable if covered with the graphene (Riso et al. 2015; Cuevas et al. 2016; Naserpour et al. 2017; Fesenko et al. 2018). Nanoscale dimensions of such beam-sensor antenna elements help reduce distortion to the electron beam velocity and power, which therefore can be assumed fixed. Under such assumption, called *fixed-current approximation*, one can perform engineering analysis of the beam monitors like it is done in the traditional antenna theory: DR can be treated as the wave scattering phenomenon.

In this work, we apply the outlined approach to study the optical DR in the presence of circular silver and dielectric nanowires as the simplest nanocavities. Some preliminary results of this analysis, however only for a dielectric wire, were presented in the contributed conference paper (Yevtushenko et al. 2018). In following, we explain the details of

Fig. 1 Cross-sectional geometry of an electron beam moving near a circular dielectric nanowire



derivations, formulate better grounded conclusions, and support them with comprehensive numerical results.

2 Scattering configuration and beam field

We assume that two-dimensional (2-D) electron beam with the harmonic time dependence $e^{-i\omega t}$ is moving over a circular dielectric nanowire with radius a , and dielectric permeability ε at the distance h from it's surface. Hence, the beam distance from the x -axis is $p = h + a$. Besides, we denote the inner and the outer domains of the wire as domains (1) and (2), respectively, and introduce the Cartesian and the polar coordinates as shown in Fig. 1.

Consider the diffraction radiation, which accompanies uniform motion of a plane unbounded electron beam along the straight trajectory with fixed velocity $v = \beta c (\beta < 1)$ near the dielectric wire. If the charge density function is modulated in time in the harmonic manner, then it is given by

$$\rho = \rho_0 \delta(y - p) \exp[i(kx/\beta - \omega t)], \quad (1)$$

where $\delta(\cdot)$ is the Dirac delta function, ω and ρ_0 are the frequency and the amplitude of beam modulation, $k = \omega/c$ is the free-space wavenumber, and c is the light velocity.

We will consider the electromagnetic-field problem in the given-current approximation. In this case the incident wave is the field of the sheet current beam (1) moving in the free space. As it was shown in van den Berg (1973), this field has the form of a slow inhomogeneous plane wave of the surface nature, the only nonzero component of the magnetic field of which is

$$H_z(x, y) = A \operatorname{sign}(y - p) e^{-q|y-p|} e^{i(k/\beta)x} \quad (2)$$

where $q = k\gamma/\beta$, $\gamma = (1 - \beta^2)^{1/2}$, function $\operatorname{sign}(y - p)$ is the sign of the expression in the brackets, time dependence is omitted, and A is a constant. This is a surface wave running along the beam trajectory in the positive direction of the x -axis.

Note that finite thickness of electron beam can be taken into account following the considerations of Palocz and Oliner (1965). In that case the beam is viewed as a velocity-dependent and frequency-dependent anisotropic dielectric slab, with the corresponding boundary conditions at the interfaces. The modulation of the electron beam can be achieved by its preliminary bunching in periodic waveguide or through direct modulation by a laser emission (Potylitsyn 1998; Talebi 2017).

3 Problem formulation

In the presence of the scatterer, the total field in the external medium is characterized by the sum $H_z^{tot} = H_z^{in} + H_z^{(2)}$. In addition, in the scatterer the field $H_z^{(1)}$ is different from (2).

The unknown field function must satisfy the conditions:

1. The Helmholtz equation with coefficient $k_1 = \alpha k$ in domain (1) and $k_2 = k = \omega/c$ in domain (2),

$$(\Delta + k_{1,2}^2)H^{(1,2)}(\vec{r}) = 0 \tag{3}$$

2. The boundary conditions at $r = a$ and $0 \leq \varphi < 2\pi$,

$$H_z^{(1)} = H_z^{in} + H_z^{(2)}, \quad E_\varphi^{(1)} = E_\varphi^{in} + E_\varphi^{(2)}; \tag{4}$$

note that from Maxwell’s equations it follows that

$$E_\varphi^{(1,2)} = Z_0(ik\varepsilon_{1,2})^{-1} \partial H_z^{(1,2)} / \partial r, \tag{5}$$

where the polar coordinates (r, φ) relate to the Cartesian ones as $x, y = r(\cos, \sin)\varphi$ and $Z_0 = (\mu_0/\varepsilon_0)^{1/2}$ is vacuum impedance,

3. The condition for the local power finiteness,

4. The radiation condition at infinity (outgoing wave behavior),

$$H_z^{(2)}(r, \varphi) \sim 2^{1/2}(i\pi k_2 r)^{-1/2} e^{ik_2 r} \Phi(\varphi) \quad \text{at } r \rightarrow \infty, \tag{6}$$

These conditions guarantee the solution uniqueness.

4 Basic equations

The circular shape of the boundaries between different materials suggests the use of the method of separation of variables. This means we expand the field functions in each domain in terms of Fourier series in the angular coordinate φ , in particular, if $r \sin \varphi < p$ and $r > a$ then

$$H_z^{in}(\vec{r}) = -Ae^{-q\rho} e^{ikr \cos(\varphi+\psi)}, \tag{7}$$

where we introduce the complex incidence angle ψ , such that

$$\cos \psi = 1/\beta, \quad \sin \psi = i\gamma/\beta, \tag{8}$$

and, according to the Anger formula, obtain

$$H_z^{in}(\vec{r}) = -Ae^{-q(h+a)} \sum_{m=-\infty}^{+\infty} i^m J_m(kr)(1 - \gamma)^m \beta^{-m} e^{im\varphi} \tag{9}$$

The scattered field is expressed as

$$H_z^{sc}(\vec{r}) = \sum_{m=-\infty}^{+\infty} \left\{ \begin{array}{l} a_m J_m(k_1 r), \quad r < a \\ b_m H_m^{(1)}(kr), \quad r > a \end{array} \right\} e^{im\varphi}, \tag{10}$$

where a_m, b_m are unknown coefficients and J_m and $H_m^{(1)}$ are the Bessel and Hankel (first kind) functions. The coefficients are found using the conditions 1–4 in analytical form as

$$a_m = C [f_m(ka)H'_m(ka) - H_m(ka)f'_m(ka)] (\Delta_m)^{-1}, \tag{11}$$

$$b_m = C [f_m(ka)\alpha J'_m(k\alpha a) - J_m(k\alpha a)f'_m(ka)] (\Delta_m)^{-1}, \tag{12}$$

where the superscripts of the Hankel functions and their derivatives are omitted, and other notations are

$$C = -Ae^{-q(h+a)}, \tag{13}$$

$$f_m = i^m J_m(ka)(1 - \gamma)^m \beta^{-m}, \quad f'_m = i^m J'_m(ka)(1 - \gamma)^m \beta^{-m}, \tag{14}$$

$$\Delta_m = J_m(k\alpha a)H'_m(ka) - \alpha J'_m(k\alpha a)H_m(ka), \tag{15}$$

Here, characteristic equations of the considered scatterer,

$$\Delta_m(k) = 0, \quad m = 0, \pm 1, \pm 2, \dots, \tag{16}$$

may have only complex solutions, k_{mn} , which form a discrete set with negative imaginary parts. These are complex natural wavenumbers of the modes of dielectric wire as open cavity, usually denoted as $H_{m,n}$ where $m = 0, 1, \dots$ and $n = 1, 2, \dots$

We characterize the scatterer with its total scattering cross-sections (TSCS) (17) and absorption cross-sections (ACS). TSCS is the result of integration of the Poynting vector flux of the scattered field over all space directions,

$$\sigma_{sc} = \frac{4}{kA^2} \sum_{m=-\infty}^{+\infty} |b_m|^2, \tag{17}$$

ACS is obtained with the aid of the Optical Theorem (a.k.a Complex Poynting Theorem) applied to the total field function and its complex conjugate. With account of (8), it takes form of

$$\sigma_{abs} = -\frac{4}{kA^2} e^{-qp} \operatorname{Re} \sum_{m=-\infty}^{+\infty} i^m b_m \left(\frac{1 - \gamma}{\beta} \right)^m - \sigma_{sc} \tag{18}$$

Presented further results for (17) and (18) are normalized by $4a$ that is the limit value of σ_{sc} at $\beta = 1$ and $a/\lambda \rightarrow \infty$.

5 Numerical results

We have studied the DR characteristics for the scatterer shaped as a circular dielectric wire shown in Fig. 1.

The plots in Fig. 2 demonstrate the dependences of the normalized TSCS on the modulation wavelength in the visible range, for the silicon wire with the radius 50 nm, relative dielectric constant $\epsilon = 12$, the separation distance $h = 10$ nm, and several values of the relative beam velocity β . As one can see, due to rather high optical contrast of silicon, even such a tiny wire behaves as an open nanocavity.

Indeed, for all values of the relative beam velocity β the spectra of TSCS display three distinctive peaks in the visible and ultra-violet ranges. Their wavelengths positions at 464 nm, 306 nm, and 225 nm do not depend on the relative beam velocity β .

To clarify the nature of these peaks of TSCS, we have calculated the complex eigenvalues of the dielectric nanowire. They are presented in Fig. 3. There are four modes which have their wavelength between 150 and 900 nm. The most "blue" of them, $H_{2,1}$, has the largest Q-factor. The mode denoted XH_1 corresponds to the so-called external mode of a

Fig. 2 Normalized TSCS of the 50-nm in radius lossless silicon nanowire ($\epsilon = 12$) versus the wavelength in the visible range, for several values of the electron relative velocity β . Note the resonances on the wire modes

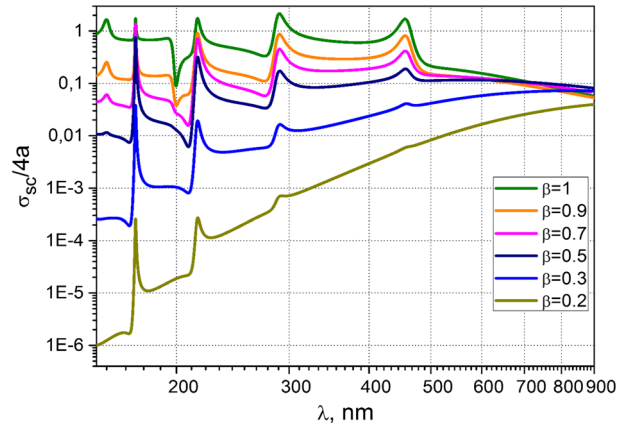
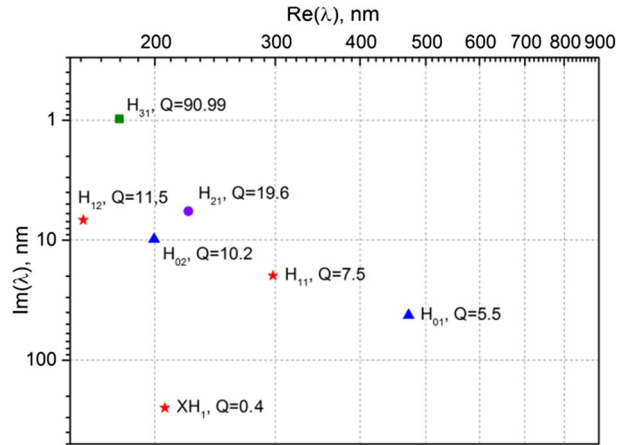


Fig. 3 Complex eigenvalues of the 50-nm in radius lossless silicon nanowire in the visible range



circular dielectric cylinder, the existence of which was mentioned, for instance, in Dettmann et al. (2009). They have very low Q-factors and do not produce any distinctive peaks in the spectra of TSCS and ACS. Other internal modes with high Q-factors are found in the deep ultraviolet range below 200 nm. The near field patterns of the internal modes with complex eigenvalues are presented in Fig. 4.

The panels of Fig. 5 show the in-resonance near field patterns for the same dielectric nanowire as in Fig. 2 and two values of β . One can clearly see the straight trajectory of the beam at the distance $h = 10$ nm above the wire. The bright spots of the field inside the wire enable one to identify the resonating modes. The lowest of them, in frequency, is the H_{01} mode at 464 nm that is certified by the single bright spot near to wire’s center. The next, in frequency, is the dipole mode H_{11} at 306 nm showing two bright spots. The most high-frequency peak at 225 nm is on the quadrupole mode H_{21} . This field pattern is well visible for the relativistic beam DR, as at $1 - \beta \ll 1$ the beam field (2) is very close to a plane wave, albeit with a jump at the beam trajectory.

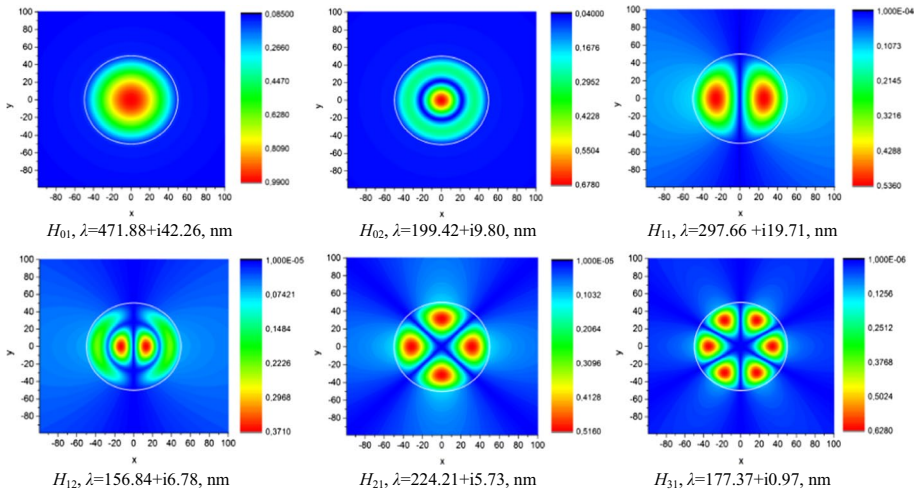


Fig. 4 Near field patterns of the lowest-order internal eigenmodes of 50-nm in radius silicon nanowire with the wavelengths between 150 and 900 nm

Here, it is necessary to remind that if $\beta \neq 0$ the incident field (2) is not symmetric with respect to the wire section by the x -axis. Indeed, for instance, the field (10) inside the wire can be rewritten as

$$H_z^{sc}(\vec{r}) = \frac{2C}{\pi ka} \sum_{m=0}^{\infty} i^m J_m(k_1 r) [B_m^+ \cos m\varphi + iB_m^- \sin m\varphi], \tag{19}$$

where

$$B_m^\pm(\beta) = [(1 - \gamma)^m \pm (1 + \gamma)^m] \beta^{-m} \tag{20}$$

Therefore, at the resonance wavelengths, the beam field excites not a single one of two degenerate wire modes $H_{m,n}$ ($m > 0$) but the both, and the contribution of the anti-symmetric with respect to $y=0$ component gets larger with smaller β . This leads to the overlap of two modal patterns so that the resulting field portrait resembles a continuous ring. The reason is that if $\beta \ll 1$ (non-relativistic beam) then $B_m^\pm(\beta) = \pm (2/\beta)^m [1 + O(\beta^2)]$. Hence the inner field pattern takes the form of the rotating wave, $J_m(kaa)(\cos m\varphi - i \sin m\varphi) + O(\beta)$, instead of the standing-wave $J_m(kaa) \cos m\varphi$, observed in the plane wave scattering.

This feature is also well visible in the far zone, where the normalized by maximum value angular scattering patterns are also shown in Fig. 5 at the same wavelengths. If $\beta \ll 1$, then the in-resonance radiation becomes omnidirectional. Note that this is not true for the resonance on the H_{01} mode (Fig. 5a, b) because in this case the contribution of anti-symmetric field component is close to zero.

We have also studied the DR characteristics of the same beam (1) moving near a circular metal (silver) nanowire. The complex-valued bulk dielectric permittivity of silver has been taken from the paper of Johnson and Christy (1972) and combined with a cubic spline interpolation (Fig. 6). In computations, the associated series have been truncated at the number ± 10 that well exceeds the maximum of the values ka and $ka|\epsilon|$ in the whole optical range and provides 6 and more correct digits.

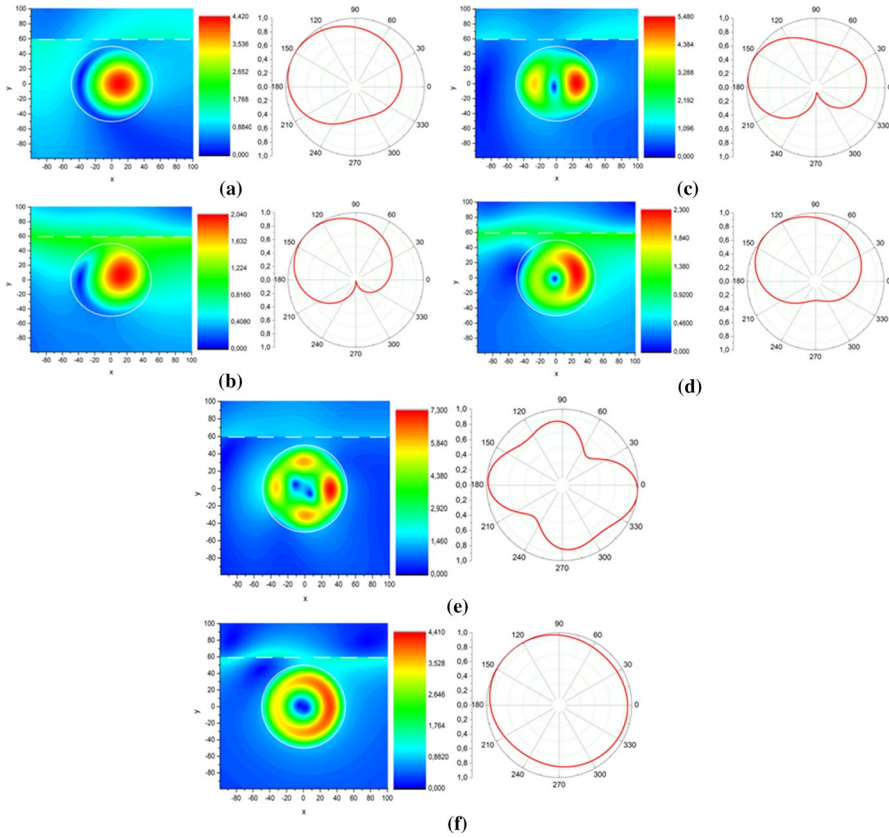
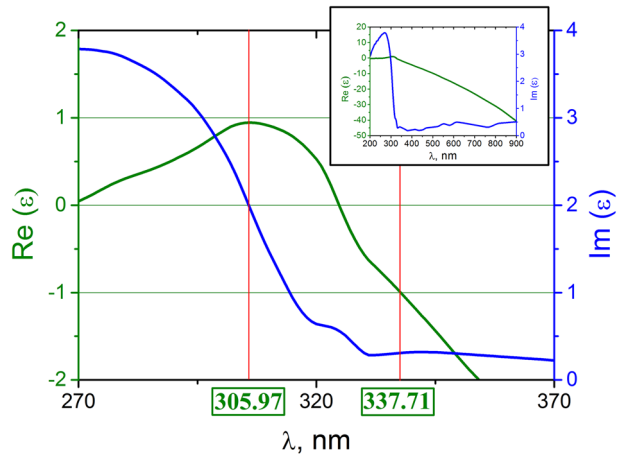


Fig. 5 Total near magnetic field patterns (left panels) and normalized far-field scattering patterns (right panels) of the lossless silicon nanowire of the radius $a=50$ nm and $\beta=0.9$ (**a, c, e**), $\beta=0.5$ (**b, d, f**) in the resonances on the modes H_{01} for $\lambda=464$ nm (**a, b**), H_{11} at $\lambda=306$ nm (**c, d**) and H_{21} at $\lambda=225$ nm (**e, f**)

Fig. 6 Complex permittivity function of silver as a function of the wavelength in the visible range



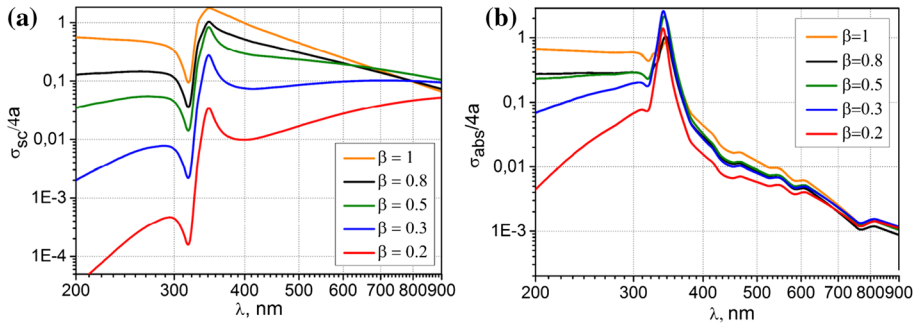


Fig. 7 Normalized TSCS (a) and ACS (b) of the 50-nm in radius silver nanowire versus the wavelength in the visible range, for several values of the electron relative velocity β

Note that the silver nanowire's dielectric function varies between 0.93 (at $\lambda=306$ nm) and -40 in the visible range and that the losses are quite considerable, between 0.2 and 3.9.

The plots in Fig. 7 demonstrate the dependences of the normalized TSCS and ACS on the modulation wavelength in the visible range, for the wire with the radius 50 nm, the separation distance $h=10$ nm, and several values of the relative beam velocity β . For all β , the plots of TSCS show the maximum at $\lambda=347$ nm preceded by the minimum at $\lambda=318$ nm and the plots of ACS—at $\lambda=343$ nm. Note that ACS is quite comparable with TSCS, especially in the blue and violet parts of the spectrum.

As expected, the wavelengths of the peak scattering and peak absorption are very close to the root of the “textbook” quasi-static equation, $\text{Re } \epsilon(\lambda) = -1$ (Bohren and Huffman 2004; Velichko and Natarov 2018), found at $\lambda=338$ nm (Johnson and Christy 1972). This is a collective resonance caused by the infinite number ($m=1, 2, \dots$) of the transverse LSP modes of a circular wire with negative dielectric function, because if $a/\lambda \rightarrow 0$, then $\Delta_m(\lambda) \approx \epsilon(\lambda) + 1 + O(m^{-1}a^2\lambda^{-2})$ (Velichko and Natarov 2018). The peaks of separate LSP resonances merge together because of the losses in silver.

The minimum of TSCS (and to lesser extent of ACS) is typical for the plasmonic scatterers, see Cuevas et al. (2016), Naserpour et al. (2017), Fesenko et al. (2018) and Yevtushenko et al. (2018). Its location in wavelength corresponds to the value, at which the dielectric function of silver comes near to 1, $\text{Re } \epsilon(\lambda) = 1$. Here the metal placed in the vacuum becomes optically transparent although still not invisible due to small absorption. According to Johnson and Christy (1972), that happens at $\lambda=308$ nm, and the red shift of the minimum in Fig. 7 is the effect of the finite wire radius. As can be found after inspection of the works (Byelobrov et al. 2012; Natarov et al. 2014a, b; Zinenko et al. 2016), this “invisibility” effect is equally well observable in the scattering of light by finite and infinite arrays of circular silver nanowires. Potentially such optical transparency can be also useful in the design of beam velocity sensors.

To clarify the nature of the peak of TSCS, we have calculated the complex eigenvalues of the silver nanowire using the rigorous characteristic Eq. (15). Here, Johnson and Christy data for $\epsilon(\lambda)$ cannot be used directly because they were measured for the real frequencies. To overcome this difficulty, we have used the modified Drude+two Lorentzians formula presented in Vial and Laroche (2008) that provides reasonably good

Fig. 8 Complex wavelengths of plasmon eigenmodes of the 50-nm in radius silver nanowire in the visible range

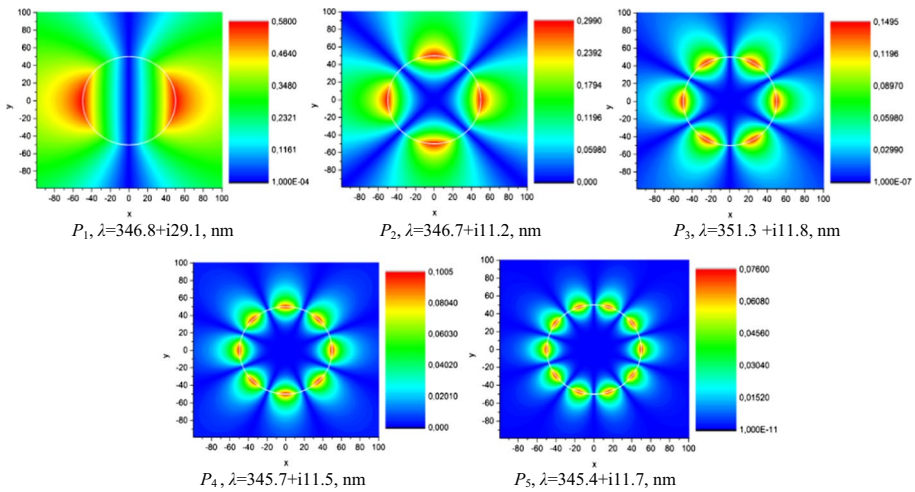
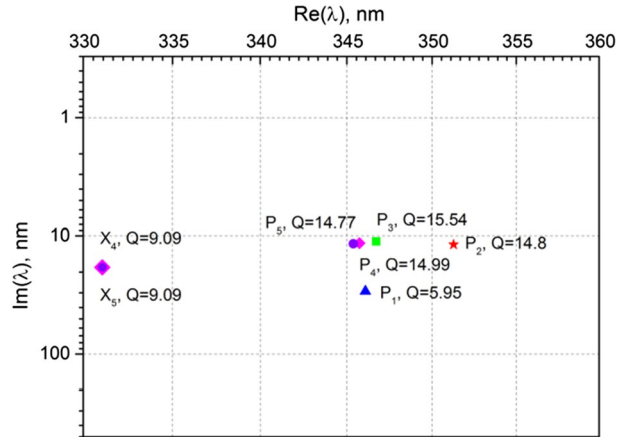


Fig. 9 Near field patterns of the lowest-order plasmon eigenmodes of the 50-nm in radius silver nanowire with the wavelengths between 330 and 350 nm

approximation of the measured data in the range between 200 and 400 nm, and continued it to the complex frequencies.

The results are presented in Fig. 8. As expected, for all m the complex wavelengths of the plasmon eigenmodes P_m are located between 330 and 360 nm and have similar imaginary parts of λ . Their Q-factors are between 5 and 15. They correspond to the localized plasmon modes of the metal wire P_1 to P_5 . The notations X_4 and X_5 correspond to the so-called secondary plasmon modes, the existence of which was apparently mentioned first time in Natarov (2014). They have comparable Q-factors however produce very small peaks in the spectra of TSCS and ACS. The near field patterns of the plasmon modes P_1 to P_5 are presented in Fig. 9.

We have also computed the total near magnetic field patterns and the normalized DR far-field angular scattering patterns of the same silver nanowire excited by the beam of particles (1), at the fixed values of β and λ . As one can see in Fig. 10, at the resonance

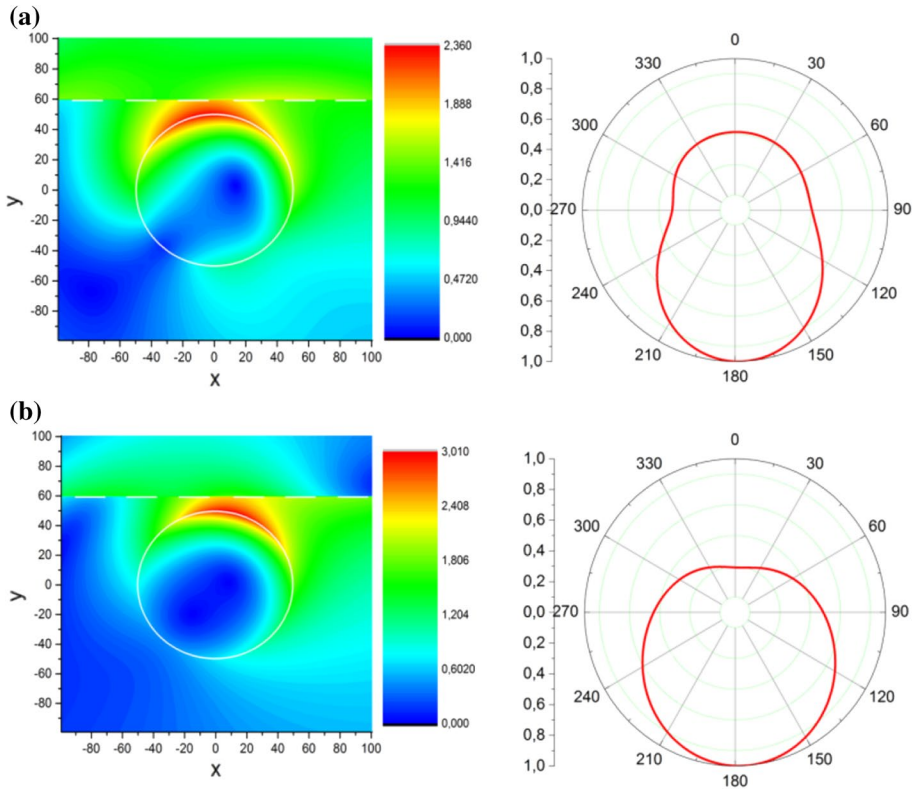


Fig. 10 Near magnetic field patterns (left) and normalized far-field scattering pattern (right) of the silver nanowire of the radius $a = 50$ nm for $\beta = 0.8$ (a), $\beta = 0.5$ (b) in the collective LSP resonance at $\lambda = 347$ nm

wavelengths the total field is dominated by the field of the corresponding plasmon mode. Its bright spots are located near the surface of the nanowire and do not penetrate into it. This is explained by the surface nature of the plasmon modes.

At the “invisibility wavelength” of $\lambda = 318$ nm, the total field in the near zone shows the beam field (2) only slightly perturbed by the wire—see Fig. 11.

The shape of the far-field DR patterns can be explained by the contribution of the field part, which is anti-symmetric with respect to the wire center (along the y -axis). Its maximum is always oriented in the normal direction to the beam trajectory.

6 Conclusions

If one can neglect the action of the field on the electrons, then the electromagnetic field of a modulated 2-D beam takes form of a surface wave propagating along the beam trajectory. This wave induces the polarization and surface currents on the local obstacles and hence a radiation occurs even if the beam does not touch the obstacle. In fact, an obstacle plays the role of optical nanoantenna, which makes the beam of particles visible. As we have shown, a nanowire behaves as an open resonator, thanks to which the radiated power is enhanced near the natural-mode wavelengths.

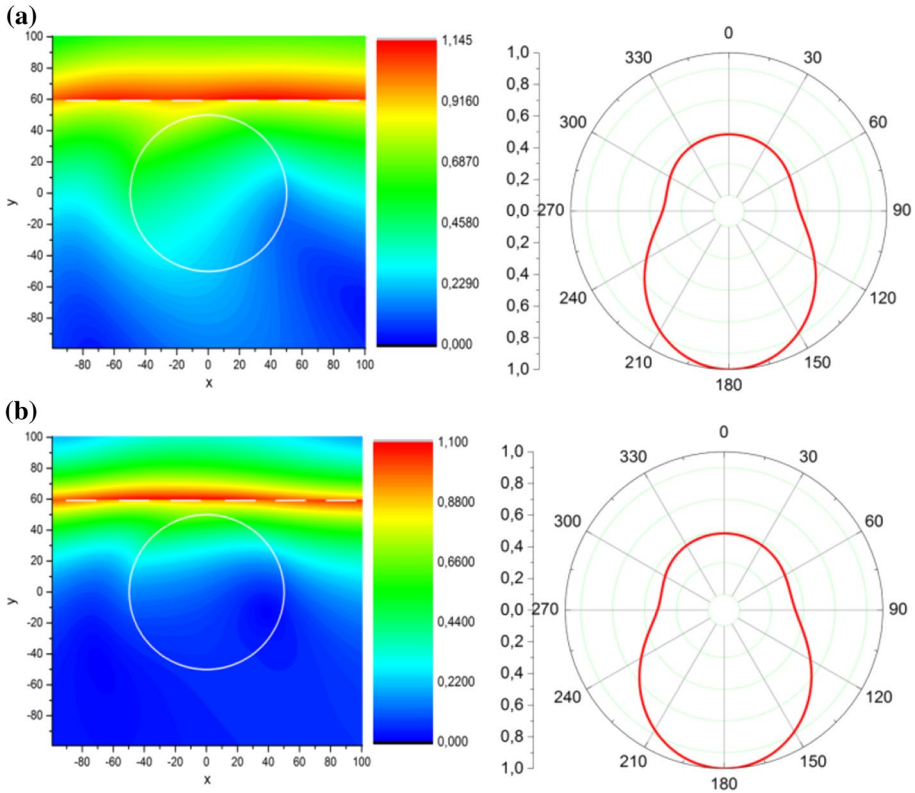


Fig. 11 “Invisibility effect:” the same as in Fig. 10 however at $\lambda = 318$ nm in the minimum of TSCS plots

For the dielectric nanowire, unlike the more conventional plane-wave scattering, the in-resonance fields (except of the resonance on the H_{01} mode) are shaped as rotating cylindrical waves. This happens because of three circumstances: (1) the beam field depends on y , and hence there are no “dark modes” of the wire that remain not excited because of orthogonal symmetry with respect to the incident wave, (2) the symmetric and the anti-symmetric natural modes of the wire remain degenerate, and (3) if $\beta \rightarrow 0$, then the phase shift between two field components becomes $\pi/2$.

We also have studied, in the same framework, the optical diffraction radiation that accompanies the motion of the charged-particle beam near a plasmonic silver nanowire. As we have shown, both the radiated and the absorbed powers are enhanced near the natural-mode wavelengths of the plasmonic nanowire open resonator. In this case, in-resonance fields are shaped as rotating surface cylindrical waves made of two degenerate LSP modes with nearly $\pi/2$ phase shift. The obtained results can be useful for monitoring of variation of beam parameters. Unlike the diffraction radiation in the presence of a dielectric nanowire, a metal nanowire placed in vacuum also displays the effect of “invisibility” at the wavelength close to the optical transparency of metal.

Acknowledgements The first author acknowledges, with gratitude, the support of the IEEE Antennas and Propagation Society in the form of Pre-Doctoral Research Award.

References

- Baryshevsky, V.G., Gurnevich, E.A.: Cherenkov and parametric (quasi-Cherenkov) radiation produced by a relativistic charged particle moving through a crystal built from metallic wires. *Nucl. Instrum. Methods B* **402**, 30–34 (2017)
- Bobb, L., Kieffer, R., et al.: Feasibility of diffraction radiation for noninvasive beam diagnostics as characterized in a storage ring. *Phys. Rev. Accel. Beams* **21**, 03801 (2018)
- Bohren, C.F., Huffman, D.R.: *Absorption and Scattering of Light by Small Particles*. Wiley-VCH Publ, Weinheim (2004)
- Byelobrov, V.O., Benson, T.M., Nosich, A.I.: Binary grating of sub-wavelength silver and quantum wires as a photonic-plasmonic lasing platform with nanoscale elements. *IEEE J. Sel. Top. Quantum Electron.* **18**(6), 1839–1846 (2012)
- Castellano, M.: A new non-intercepting beam size diagnostics using diffraction radiation from a slit. *Nucl. Instrum. Methods Phys. Res. A* **394**, 275–280 (1997)
- Castellano, M., et al.: Measurements of coherent diffraction radiation and its application for bunch length diagnostics in particle accelerators. *Phys. Rev. E* **63**, 056501 (2001)
- Cuevas, M., et al.: Complex frequencies and field distributions of localized surface plasmon modes in graphene-coated subwavelength wires. *J. Quant. Spectrosc. Radiat. Transf.* **173**, 26–33 (2016)
- Dettmann, C.P., Morozov, G.V., Sieber, M., Waalkens, H.: Internal and external resonances of dielectric disks. *Eur. Phys. Lett.* **87**(3), 34003 (2009)
- Fesenko, V.I., Shcherbinin, V.I., Tuz, V.R.: Multiple invisibility regions induced by symmetry breaking in a trimer of subwavelength graphene-coated nanowires. *J. Opt. Soc. Am. A* **35**(10), 1760–1768 (2018)
- Goponov, Y.A., Shatokhin, R.A., Sumitani, K.: Diffracted diffraction radiation and its application to beam diagnostics. *Nucl. Instrum. Methods Phys. Res. A* **885**, 134–138 (2018)
- Johnson, P.B., Christy, R.W.: Optical constants of the noble metals. *Phys. Rev. B* **6**(12), 4370–4378 (1972)
- Karataev, P., Araki, S., Hamatsu, R., et al.: Beam-size measurement with optical diffraction radiation at KEK accelerator test facility. *Phys. Rev. Lett.* **93**, 244802 (2004)
- Leedle, K.J., Ceballos, A., Deng, H., et al.: Dielectric laser acceleration of sub-100 keV electrons with silicon dual-pillar grating structures. *Opt. Lett.* **40**(18), 4344–4347 (2015)
- Naserpour, M., Zapata-Rodríguez, C.J., Vuković, S.M., et al.: Tunable invisibility cloaking by using isolated graphene-coated nanowires and dimers. *Sci. Rep.* **12**, 12186/14 (2017)
- Natarov, D.M.: Modes of a core-shell silver wire plasmonic nanolaser beyond the Drude formula. *J. Opt.* **16**(7), 075002 (2014)
- Natarov, D.M., Sauleau, R., Marciniak, M., Nosich, A.I.: Effect of periodicity in the resonant scattering of light by finite sparse configurations of many silver nanowires. *Plasmonics* **9**(2), 389–407 (2014a)
- Natarov, D.M., Marciniak, M., Sauleau, R., Nosich, A.I.: Seeing the order in a mess: optical signature of periodicity in a cloud of plasmonic nanowires. *Opt. Express* **22**(23), 28190–28198 (2014b)
- Nosich, A.I.: Diffraction radiation which accompanies the motion of charged particles near an open resonator. *Radiophys. Quantum Electron.* **24**(8), 696–701 (1981)
- Palocz, I., Oliner, A.A.: Leaky space-charge waves I: Cerenkov radiation. *Proc. IEEE* **53**(1), 24–36 (1965)
- Potylytsyn, A.P.: Resonant diffraction radiation and Smith–Purcell effect. *Phys. Lett. A* **238**, 112–116 (1998)
- Riso, M., Cuevas, M., Depine, R.A.: Tunable plasmonic enhancement of light scattering and absorption in graphene-coated subwavelength wires. *J. Opt.* **17**(7), 075001/8 (2015)
- Smith, S.J., Purcell, E.M.: Visible light from localized surface charges moving across a grating. *Phys. Rev.* **92**, 1069 (1953)
- Talebi, N.: Interaction of electron beams with optical nanostructures and metamaterials: from coherent photon sources towards shaping the wave function. *J. Opt.* **19**, 103001 (2017)
- van den Berg, P.M.: Smith–Purcell radiation from a line charge moving parallel to a reflection grating. *J. Opt. Soc. Am.* **63**(6), 689–698 (1973)
- Velichko, E.A., Natarov, D.M.: Localized versus delocalized surface plasmons: dual nature of resonances on a silver circular wire and a silver tube of large diameter. *J. Opt.* **20**(7), 075002/9 (2018)
- Veliev, E.I., Nosich, A.I., Shestopalov, V.P.: Radiation of an electron flux moving over a grating consisting of cylinders with longitudinal slits. *Radiophys. Quantum Electron.* **20**(3), 306–313 (1977)

- Vial, A., Laroche, T.: Comparison of gold and silver dispersion laws suitable for FDTD simulations. *Appl. Phys. B* **93**, 139–143 (2008)
- Yevtushenko, D.O., Dukhopelnikov, S.V., Odarenko, E.N., Nosich, A.I.: Optical diffraction radiation of electron beam in the presence of a dielectric nanowire resonator. In: *Proceedings of International Conference on Mathematical Methods in Electromagnetic Theory (MMET-2018)*, Kyiv, 2018, pp. 148–151
- Zinenko, T.L., Byelobrov, V.O., Marciniak, M., Ctyroky, J., Nosich, A.I.: Grating resonances on periodic arrays of sub-wavelength wires and strips: from discoveries to photonic device applications. In: Shulika, O., Sukhoivanov, I. (eds.) *Contemporary Optoelectronics: Materials, Metamaterials and Device Applications*, Ch. 4, vol. 199, pp. 65–79. Springer Series in Optical Sciences, Berlin (2016)